



## Metastable versus stable solidification of silicon cast irons, effects of magnesium and tellurium

Urko de la Torre, Anna Regordosa, Jacques Lacaze, Edurne Aguado, Jon Sertucha

### ► To cite this version:

Urko de la Torre, Anna Regordosa, Jacques Lacaze, Edurne Aguado, Jon Sertucha. Metastable versus stable solidification of silicon cast irons, effects of magnesium and tellurium. *Materialia*, 2023, 27, pp.101665. 10.1016/j.mtla.2022.101665 . hal-03920397

HAL Id: hal-03920397

<https://hal.science/hal-03920397>

Submitted on 3 Jan 2023

**HAL** is a multi-disciplinary open access archive for the deposit and dissemination of scientific research documents, whether they are published or not. The documents may come from teaching and research institutions in France or abroad, or from public or private research centers.

L'archive ouverte pluridisciplinaire **HAL**, est destinée au dépôt et à la diffusion de documents scientifiques de niveau recherche, publiés ou non, émanant des établissements d'enseignement et de recherche français ou étrangers, des laboratoires publics ou privés.

Metastable versus stable solidification of silicon cast irons,  
effects of magnesium and tellurium.

Urko de la Torre<sup>a</sup>, Anna Regordosa<sup>a</sup>, Jacques Lacaze<sup>b</sup>, Edurne Aguado<sup>a</sup>, Jon Sertucha<sup>a</sup>

a. Azterlan, Basque Research and Technology Alliance, Aliendalde Auzunea 6, E-48200 Durango (Bizkaia), Spain.

b. CIRIMAT, Université de Toulouse, CS 44362, 31030 Toulouse, France

UT : [urkodltugarte@hotmail.com](mailto:urkodltugarte@hotmail.com)

AR : [aregordosa@azterlan.es](mailto:aregordosa@azterlan.es)

JL: [Jacques.lacaze@ensiacet.fr](mailto:Jacques.lacaze@ensiacet.fr)

EA: [eaguado@azterlan.es](mailto:eaguado@azterlan.es)

JS: [jsertucha@azterlan.es](mailto:jsertucha@azterlan.es)

Corresponding author: Jacques Lacaze. Phone: +33-534323415

## Abstract

Cast iron is a material with a unique combination of design flexibility, mechanical properties, wear resistance, recyclability, low life cycle energy consumption and low cost. The optimization of current production and the development of new material variants with improved properties rely on the control of the melt throughout the process, from charge selection to casting. Thermal analysis just prior to pouring the molds has been developed over the years for melt control, e.g., for composition verification or for graphite shape prediction. Since minor additions of tellurium prevent graphite growth, thermal analysis with Te-coated cups is commonly used for compositional control of slightly hypereutectic alloys. The present study was designed to test the feasibility of using Te-coated cups to monitor the magnesium content of melts after a full or partial spheroidizing treatment leading to spheroidal or compact graphite, respectively. In the course of this work, it was realized that thermal analysis could give unreliable results when the microstructure of the casting is not homogeneous, i.e., it exhibits a mixture of metastable and stable eutectics. Tellurium has been shown to have an ambivalent effect on solidification of Mg-bearing melts.

**Keywords:** thermal analysis, solidification, cast iron, microstructure, metastable eutectic

## **1. Introduction**

Silicon cast irons are essentially Fe-C-Si alloys with 1-5 wt% silicon and containing enough carbon to give a significant amount of eutectic. At low silicon content, they tend to solidify in the metastable system in which the carbon-rich phase is  $\text{Fe}_3\text{C}$  cementite, resulting in parts that are brittle but can be made malleable by graphitization heat treatment, or can be used as is for wear resistance applications. As the silicon content increases, the temperature difference between the stable and metastable eutectic increases from 6°C in the binary Fe-C system to nearly 100°C at 5 wt.% Si (see for example the recent review in [1]). Therefore, the stable eutectic, in which the carbon-rich phase is graphite, becomes increasingly prevalent.

The competition between the two systems is of paramount importance and is often used as a classic example of the effects of nucleation and growth kinetics of the phases involved during solidification of a sample or casting [2]. While inoculation of the melt to facilitate graphite precipitation promotes solidification in the stable system, uninoculated low-silicon melts typically exhibit a metastable eutectic. The transition from stable to metastable solidification is also controlled by the cooling rate. This is used in the chill test (see review by Fras et al. [3]), in which a wedge-shaped sample is cast and begins to solidify at the apex in the metastable system until the cooling rate is reduced sufficiently for stable eutectic solidification, i.e., when there is sufficient time for nucleation and graphite growth.

The transition from the stable to the metastable system at increasing cooling rate, as well as the reverse transition at decreasing cooling rate, was studied by Magnin and Kurz [4] on laboratory samples of directionally solidified Fe-C and low-alloyed Fe-C-X alloys (X=Si, P, Cr, Mn, Ti, Al, S). The results have been discussed [5] in relation to theoretical work on eutectic growth [6]. Another similar laboratory work worth mentioning is the study by Verhoeven et al. [7, 8] of tellurium-doped Fe-C-Si alloys. These studies showed a hysteresis of the transition, so that there is a temperature range in which either structure can develop. This hysteresis results from the fact that the nucleation of graphite is easier than that of cementite, while the growth of cementite is much faster than that of graphite. For this reason, the solidification of small or medium castings can be complicated by the reversal of the microstructure from expectations (so-called inverse greyness and inverse chill), as described by Hillert and Subba Rao [9].

Hillert and Subba Rao related the solidification microstructure to thermal arrests recorded by a thermocouple located in the center of a casting, as used in thermal analysis which was a rapidly developing technique at that time [10, 11]. Further developments have been regularly described [12, 13] and thermal analysis is now used for melt and processing control, inoculation optimization and microstructure prediction, etc. A number of modeling and simulation approaches have addressed the transition from stable to metastable solidification of cast irons, applied for example to thermal analysis [14] or wedge casting [15].

The present study considers the effect of Te on the solidification behavior of cast iron with variable magnesium content using tellurium-coated cups. Such cups are typically used for compositional control of cast irons that have not been spheroidized because tellurium inhibits graphite growth [16, 17], resulting in solidification in the metastable system whose eutectic temperature depends on the silicon content [18, 19]. In the present work, a wide variety of cooling curves were obtained by holding a melt for hours in a pressurized unit so that its magnesium content slowly diminished, leading to a continuous change in the Mg/Te ratio associated with a nonmonotonic evolution of the cooling curves. The microstructure of the samples was characterized and related to the thermal records, highlighting cases where the thermal analysis does not give adequate information on the microstructure.

## 2. Experimental methodology

An uninoculated melt, prepared for casting spheroidal graphite cast iron, was maintained for 8 hours in a pressurized unit of four tons capacity after production ended. Full details of the procedure have been described for earlier test series [20, 21]. Every 30 minutes or so, a medal for chemical analysis and a series of thermal cups were cast, from which the Te-coated cup was selected for the present work. Figure 1-a shows a schematic of a cup whose cavity has a lower base of 35x35 mm, an upper base of 37x37 mm and a height of 40 mm. In total, a series of 18 melt samples were progressively collected from the pouring basin (stopper area). Carbon and sulfur contents were determined by combustion analysis (LECO CS300) and the contents of other elements by spark spectrometry (SPECTROLAB). Table 1 shows the carbon, silicon and magnesium contents of the first and last castings. While the silicon content remained unchanged throughout the test, the carbon content decreased by about 0.1 wt.% and the magnesium content reduced to almost zero. Other elements measured were 0.56-0.57 wt.% Mn, 0.024-0.029 wt.% P, 0.044-0.049 wt.% Cr, less than 0.022 wt.% Ni, 0.13-0.14 wt.% Cu and 0.026 wt.% Ti.

Table 1. Casting number, time of pouring and composition (wt.%) of the first and last castings, calculated carbon equivalent CE (wt.%) and characteristic temperatures (°C) (see text).

Sample	Time of casting	C	Si	Mg	CE	$T_{EUT}$	$T_{EW}$	$T_{EW}^{cup}$
1	5:47	3.78	2.41	0.024	4.47	1162.1	1119.1	1111.1
18	14:00	3.67	2.44	0.003	4.37	1162.2	1118.6	1110.6

The carbon equivalent of the alloys was calculated as previously reported [21, 22] and its values changed from 4.47 wt.% to 4.37 wt.% (Table 1). Compared to the value of 4.34 wt.% which corresponds to the eutectic carbon content in the Fe-C binary system, all the alloys were slightly hypereutectic although increasingly close to the eutectic composition as the holding time increased. Finally, Table 1 also gives the characteristic eutectic temperatures, namely the stable eutectic temperature  $T_{EUT}$  calculated as a function of composition as described previously [21] and the metastable eutectic temperature  $T_{EW}$  calculated as a function of the silicon content of the alloy [19]. These temperatures did not change significantly during the test because the silicon content remained almost constant. It was previously observed that the metastable eutectic temperature evaluated with a standard thermal analysis cup is shifted downward by 8°C relative to  $T_{EW}$  due to undercooling of the metastable eutectic growth [19]. The magnitude of this offset is consistent with the data reported by Oldfield and Humphreys [23] for the cooling rate experienced during the thermal analysis. The corresponding temperature is noted as  $T_{EW}^{cup}$ , and its expected values are also listed in Table 1.

Figure 1-b shows an isopleth Fe-C section of the system of interest where the stable eutectic is at the intersection of the austenite and graphite liquidus. The austenite liquidus has been extrapolated to the metastable eutectic at the intersection with the  $\text{Fe}_3\text{C}$  cementite liquidus. The solidification path of a slightly hypereutectic M alloy is represented by the two successive arrows. The primary precipitation of graphite is limited by the nucleation and growth of this phase, leading to a solidification path undercooled below the graphite liquidus. When the metastable extrapolation of the austenite liquidus is reached, austenite grows rapidly, possibly together with some stable eutectic if graphite growth is not sufficiently

hindered. As cooling continues, the solidification path of the alloy then follows the austenite liquidus, eventually reaching the metastable eutectic if growth of the stable eutectic has been restricted. It is generally accepted that solidification in the metastable system results in a flat eutectic plateau. The reason for this statement, and its limitations, will be discussed in Section 3.1.

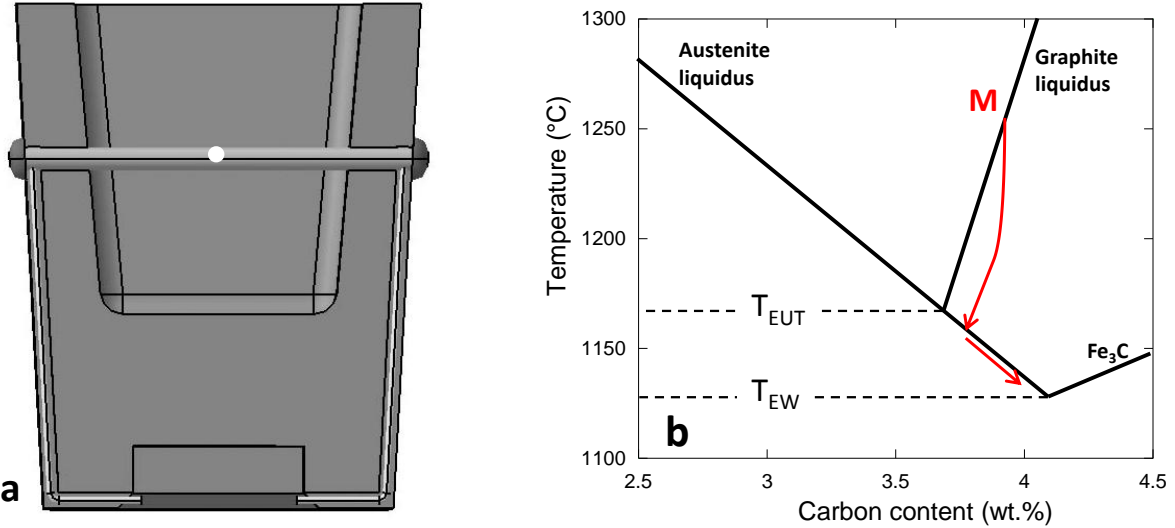


Figure 1. (a) Schematic of a cup used for thermal analysis. The thermocouple junction (white dot) is protected by a quartz tube and located in the middle of the cup cavity. (b) Fe-C isopleth section at about 2 wt.% Si. The stable  $T_{EUT}$  and metastable  $T_{EW}$  eutectic temperatures are indicated.

Unlike primary graphite precipitation which can hardly be seen on thermal analysis records of slightly hypereutectic alloys, the formation of austenite and of stable or metastable eutectic results in sufficient latent heat release to be easily detected by associated thermal arrests. All cooling curves of the cups were recorded using the Thermolan® software. The samples were then cut along a vertical plane going through the thermocouple junction and the sections were polished and prepared for metallographic observations by light microscopy and scanning electron microscopy (SEM). Optical microscopy was performed either before etching of the samples for graphite characterization or after etching with 5% Nital for carbide highlighting. The SEM used was a Quanta 200 Carl Zeiss Ultraplus equipped with a X-max 20 Oxford detector for microanalysis by energy dispersive spectrometry (EDS).

### 3. Results

#### 3.1 Thermal analysis and microstructure

Figure 2 shows the 18 records in chronological order from left to right, with an offset on the time axis for clarity. All curves show two main thermal arrests, the first short and with little or no recalescence that relates to austenite formation and is designated as  $T_{LA}$ . The  $T_{LA}$  arrest has been located on the first and last curves of figure 2. Its temperature increases from 1130°C for sample #1 to 1160°C for sample #18. The second main arrest corresponds to the eutectic reaction and takes various shapes so that the curves can be sorted into four groups according to their shape. In Figure 2, these groups are separated by the three thick curves (corresponding to samples #5, #10 and #14) and are described in more detail below.

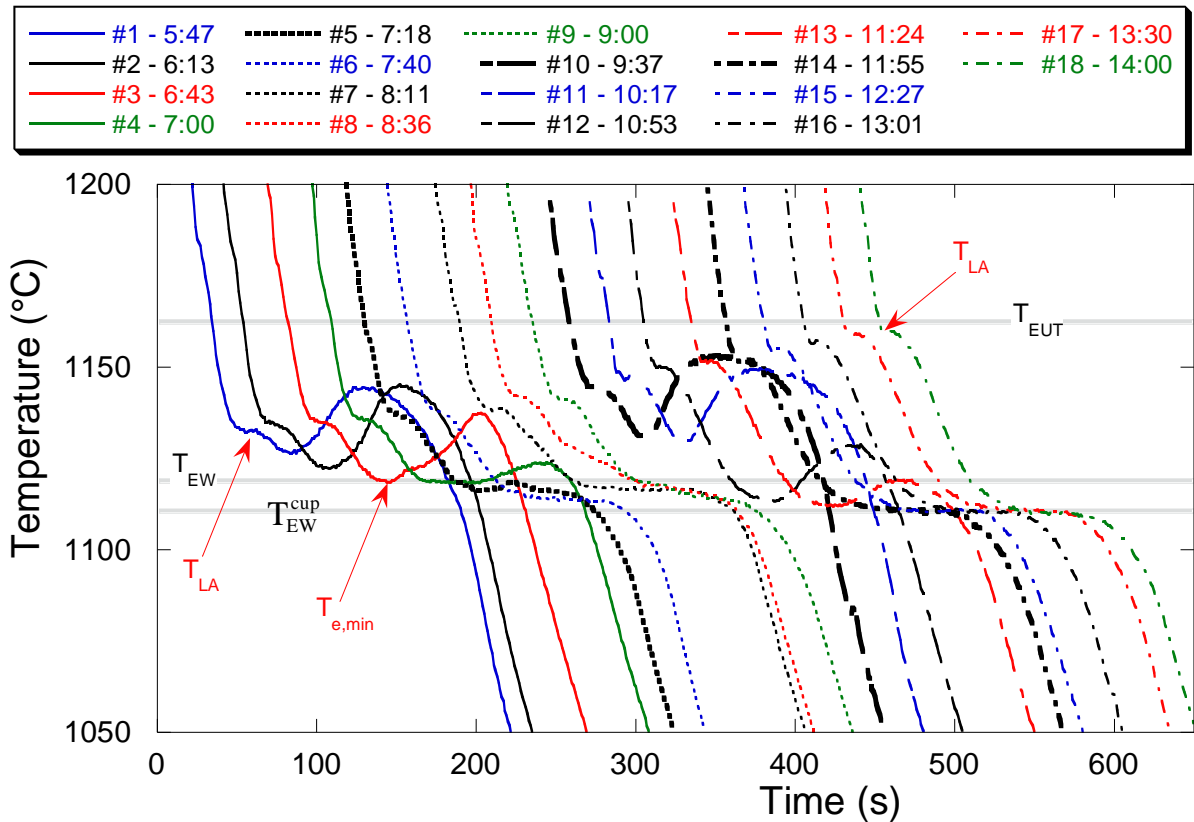


Figure 2. Set of recorded cooling curves shifted along the X axis for clarity. The reference number and time of pouring is indicated in the caption for each of the 18 castings.

The three calculated temperatures mentioned above,  $T_{EU}$ ,  $T_{EW}$  and  $T_{EW}^{cup}$ , have also been plotted in Figure 2 as horizontal gray lines whose thickness corresponds to their range of variation during the test. It can be seen that most of the  $T_{LA}$  values are well below  $T_{EUT}$ , which confirms the hypereutectic nature of the cast iron. In a previous series of similar castings,

most of the increase in  $T_{LA}$  during the test was associated with the loss of carbon during melt holding [21] and this certainly applies to the present series of castings as well. The minimum temperature before the eutectic reaction will be denoted  $T_{e,min}$  in the following and is located either above or within the temperature interval  $[T_{EW}^{cup}, T_{EW}]$ . In case of recalescence,  $T_{e,min}$  can be directly read from the cooling curve as exemplified on the record of sample #3 in figure 2. When the eutectic reaction presents a flat plateau, the characteristic  $T_{e,min}$  value is that corresponding to the local maximum of the time derivative of the cooling curve, which is often located close to the middle of the plateau.

Because of their similar shape characterized by significant eutectic recalescence, records #1 through #4 and #10 through #13 have been reproduced together in Figure 3. For such slightly hypereutectic alloys, the primary precipitation of graphite leads to no thermal arrest and it is only when austenite forms that significant latent heat is released and appears with the  $T_{LA}$  arrest [24]. As the temperature drops below  $T_{LA}$ , the graphite continues to nucleate and begins to form eutectic cells with the austenite. At some point, the latent heat release associated with the incipient eutectic reaction becomes sufficiently rapid and leads to recalescence.

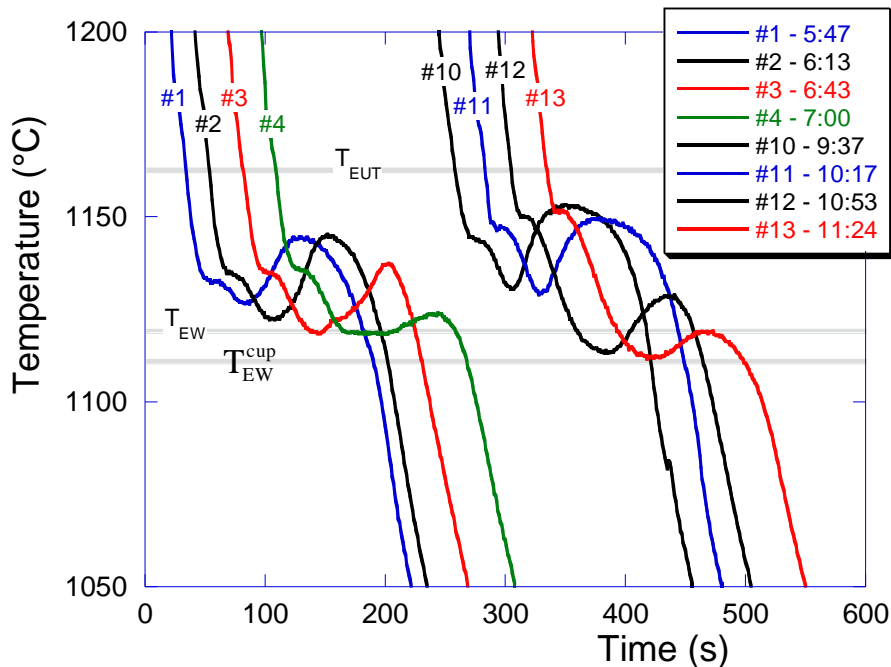


Figure 3. Records #1 through #4 and #10 through #13. The curves have been shifted along the X axis for clarity.

Curves #1, #2, #10 and #11 showed a temperature  $T_{e,min}$  above  $T_{EW}$  and it is generally accepted that the corresponding samples have a predominantly graphitic (stable eutectic) microstructure [9, 13]. If carbides are to appear in this case, it will be when the temperature falls below  $T_{EW}$  at the very end of solidification and they will be located in the last freezing zones. On the contrary, the other four curves in Figure 3 showed a temperature  $T_{e,min}$  equal to or lower than  $T_{EW}$  and it can be expected that carbides could have formed at the beginning of the eutectic reaction. However, the significant recalescence of the cups demonstrates that many stable eutectic cells also developed [25].

It seemed interesting to check the microstructure of samples #3 and #4 where the temperature  $T_{e,min}$  was equal to  $T_{EW}$  and was associated with a short plateau for sample #4. A micrograph of sample #3 is seen in Figure 4-a and shows an amount of graphite that ensures that its central part had fully solidified in the stable system. It was further verified by etching that no carbides were formed in the central part of this sample. It is interesting to note that the shape of the graphite strongly suggests that solidification took place in three successive stages: 1) formation of large, more or less spheroidal primary graphite precipitates; 2) precipitation of compacted graphite that must have formed by a coupled eutectic with austenite; 3) precipitation of fine graphite in the last zones to solidify. The shape of these fine graphite precipitates resembles the mesh graphite often observed in Te-doped cast irons (also Pb and Bi), whether spheroidized [26, 27] or not [16, 28]. The transition from step 2 to step 3 can probably explain the intermediate arrest observed on the curve of sample #3 between  $T_{e,min}$  and the maximum eutectic temperature.

In contrast, the microstructure of sample #4 seen in Figure 4-b shows well-developed cells of metastable eutectic that must have grown during the flat plateau at  $T_{e,min}=T_{EW}$  until being overtaken by growth of stable eutectic cells that led to the final recalescence. That the plateau is here at  $T_{EW}$  and not at  $T_{EW}^{cup}$  as expected will be discussed later.

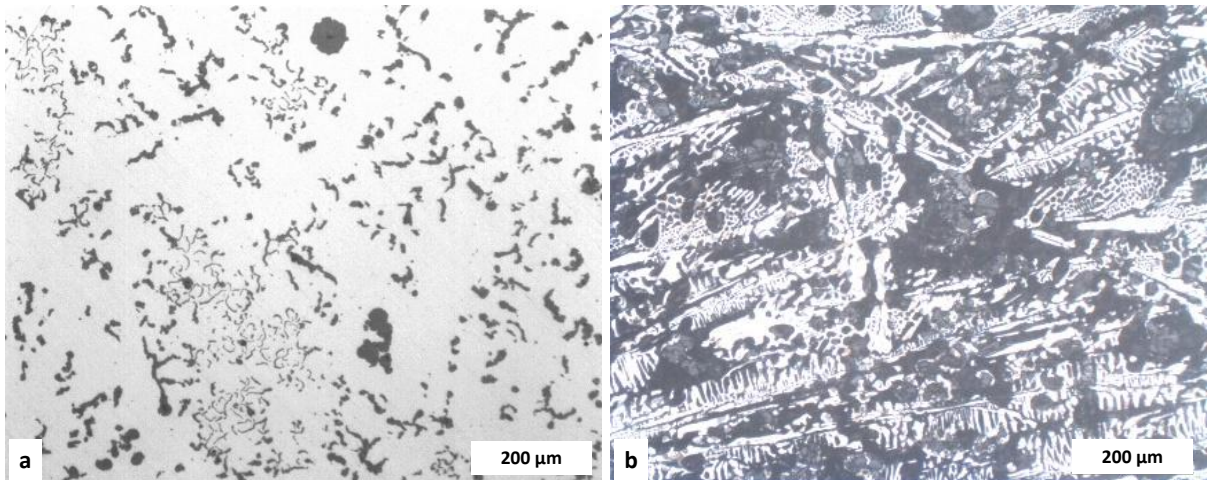


Figure 4. Micrograph of the central area of sample #3 before etching (a). After etching, sample #3 was found to be free of carbides. Micrograph of the central area of sample #4 after etching to evidence carbides that appear white (b).

The two sets of records from #1 to #4 and from #10 to #13 show the same characteristics, namely a decrease in  $T_{e,\min}$  associated with an increase (first two records) and then a decrease (last two records) in recalescence. In a similar previous study, the decrease in  $T_{e,\min}$  was understood as a continuous decrease in the number of graphite nuclei due to the decrease in magnesium, while the decrease in recalescence was due to the correlated increase in the amount of metastable eutectic [20]. The evolution with melt holding time appears to have been much faster in the #1 to #4 series than in the previous study and this could be due to the effect of tellurium on the amount of free magnesium as discussed in section 4.1. In the earlier work [19], the eutectic plateau remained flat after the recalescence disappeared. It was therefore unexpected in the present work that recalescence appeared again after samples #5 to #9 and that samples #10 to #13 showed the same behavior as samples #1 to #4. This suggested a metallographic study of sample #10 which is described below.

Figure 5-a shows half of the vertical section of the sample #10 after etching. On the upper part appears an area with a uniform gray level that corresponds to the metastable eutectic. A thin layer of metastable eutectic was also detected on the lower surface of the section while all the rest of the sample, and in particular the central part, shows rounded cells of stable eutectic. The transition between the upper area and the rest of the sample is shown in Figure 5-b and appears to be abrupt, in agreement with many observations on laboratory castings, e.g., those of Dawson [29] and Mampaey [30]. This sharpness is important when looking for surface hardening of the component upon casting [31]. Finally, Figure 5-c taken from the middle of

the sample shows that lamellar and undercooled graphite formed during solidification of the majority of the casting. These metallographic observations on the middle portion of the section are therefore in perfect agreement with the cooling curve of sample #10 that indicates that solidification occurred in the stable system. One may wonder whether the graphite nuclei required for such behavior can be related to a specific ratio of magnesium and tellurium in the melt. This question will be discussed in section 4.1.

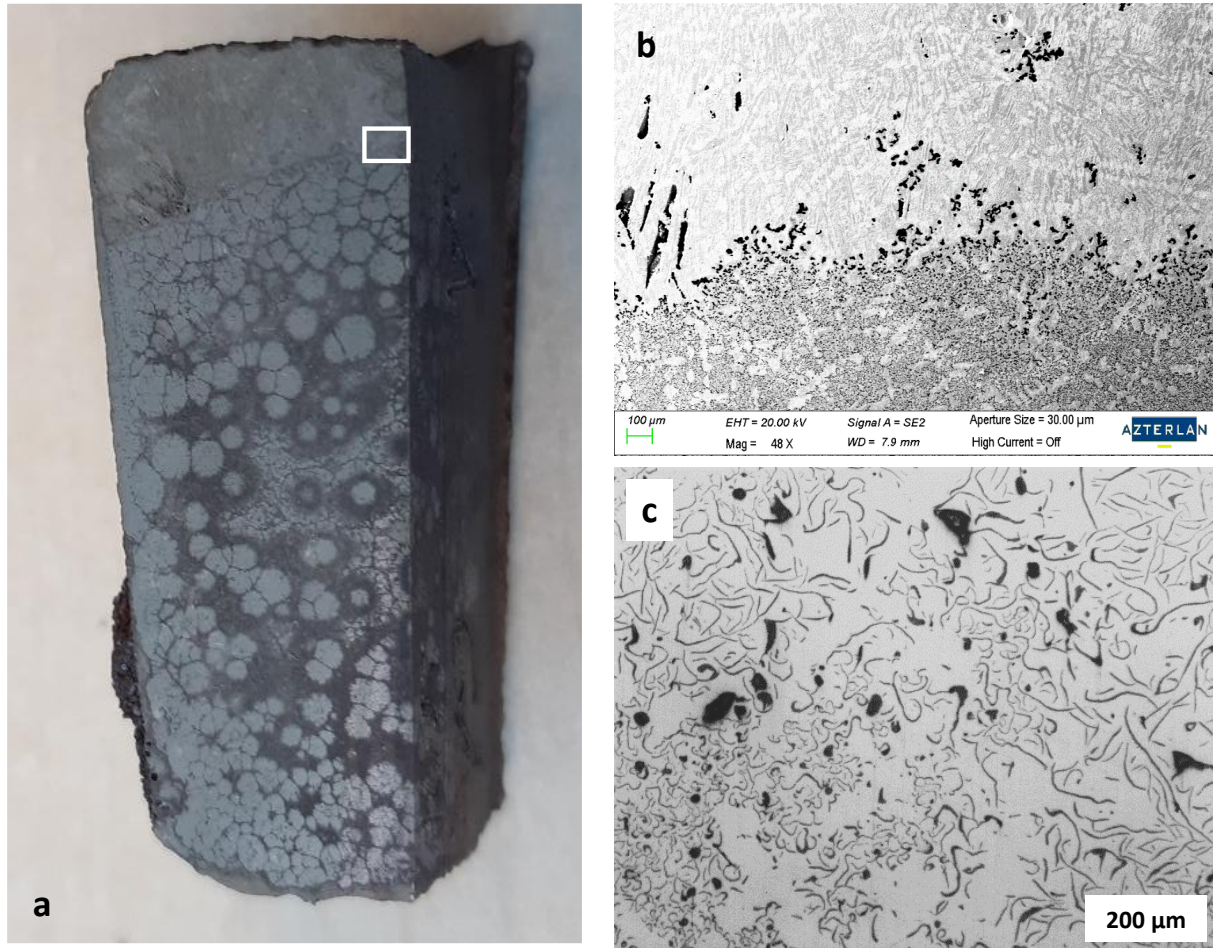


Figure 5. Metallographic observations of sample #10. a) Light macrophotography of half the vertical section of the etched sample whose height is 40 mm. b) SEM micrograph of the area marked with a rectangle in (a) showing the transition from metastable to stable solidification microstructure. c) Light micrograph of one of the round cells seen in (a). Micrographs b and c were taken before etching.

Figure 6 shows again the records of samples #5 to #9 that were obtained in the time interval between the two series examined above. Referring to our previous work [21], samples #5 through #7 with a more or less flat plateau located below  $T_{EW}$  are well in line with the

decrease of  $T_{e,\min}$  shown by the series #1 through #4 and are correlated with an increase of the amount of metastable eutectic. However, the last two samples, #8 and #9, showed unexpectedly a continuous decrease of the temperature instead of a flat plateau. Such a type of cooling curves is quite uncommon, but has been reported by Nieswaag and Zuithoff [16, 32] who performed solidification experiments under  $N_2+H_2$  atmosphere of Te-doped grey (not spheroidized) cast irons. Further, it is clearly seen that the slope just below  $T_{LA}$  for samples #7 and #8 is lower than for the other records, suggesting that numerous graphitic eutectic cells developed, in agreement with the finding of Nieswaag and Zuithoff.

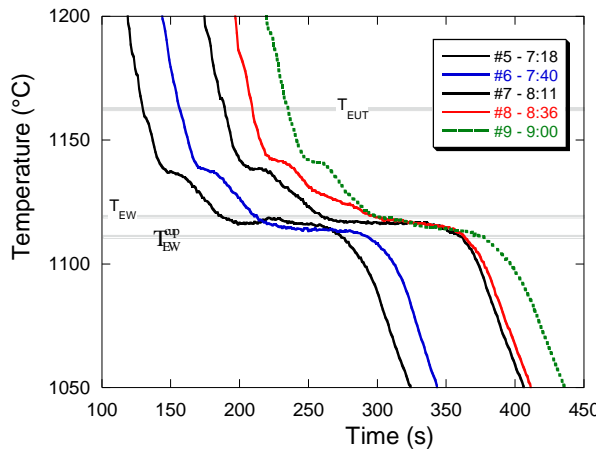


Figure 6. Temperature-time records of samples #5 to #9 shifted along the X axis for clarity.

In fact, graphite was observed in all samples of this series (#5 to #9) though intermixed with various amounts of metastable eutectic. Sample #7 was of particular interest as the amount of graphite appeared quite large in its center. Figure 7-a shows half the vertical section of the cup #7 after etching and it is clearly seen that the outer rim consists of metastable eutectic while numerous cells of stable eutectic with either lamellar or undercooled graphite appear in the central part. This microstructure is illustrated at higher enlargement in figure 7-b.

It is striking that the thermal records of samples #7 and #10 are so different while the macrographs of their sections are similar, compare figures 5-a and 7-a. The particularity of sample #7 is that it has a thick edge of metastable eutectic over its entire surface whereas this zone is limited to the upper surface of sample #10. Sample #7 is thus an important case where the thermal record gives completely wrong information about the solidification microstructure: the flat plateau under  $T_{EW}$  does not correspond to the graphitic eutectic observed in the central part of the sample. During solidification of the outer rim, the

solidification front must have been at a temperature below  $T_{EW}$  and the inner liquid was certainly strongly undercooled when graphite nuclei appeared and led to cells of stable eutectic. However, these cells were not numerous enough in sample #7 to give rise to recalescence that would have been indicative of an inhomogeneous microstructure. In other words, the comparison of samples #7 and #10 shows that the information obtained from the cooling curves can be strongly biased in the case where the microstructure is not homogeneous at the scale of the thermal analysis sample.

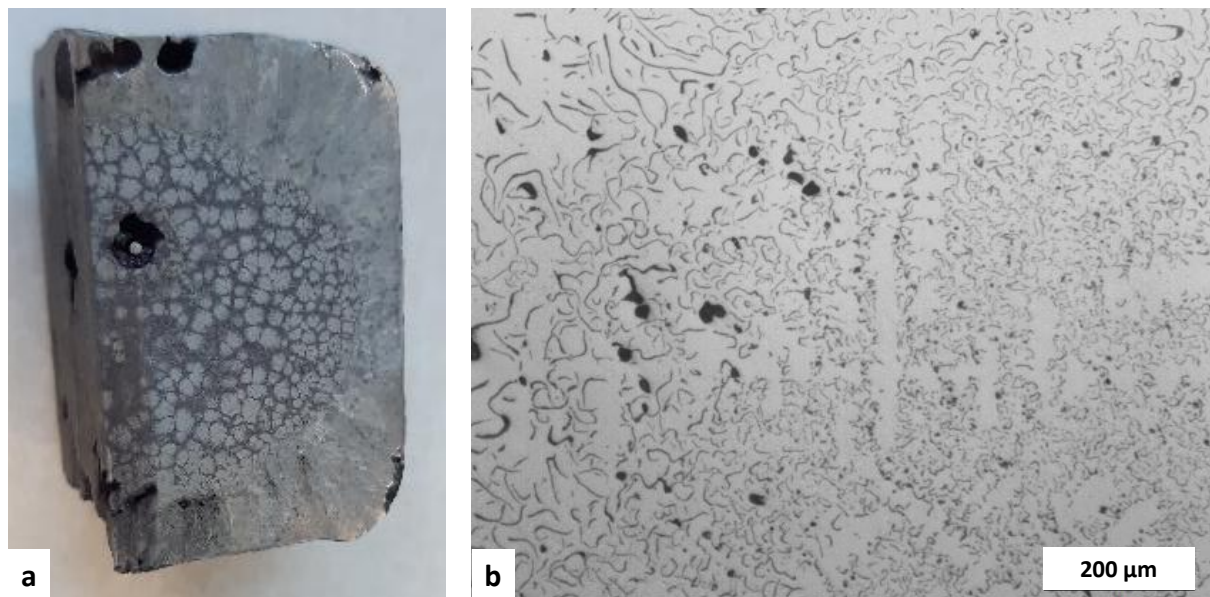


Figure 7. Metallographic observations of sample #7. a) Light macrophotography of half the vertical section of the sample whose height is 40 mm (etched). b) Light micrograph in the central area (unetched).

Finally, Figure 8 shows the thermal records of samples #14 to #18. Here, the  $T_{AL}$  arrest is slightly recalescent while the eutectic plateau is perfectly flat at  $T_{EW}^{cup}$  which is the expected temperature for the metastable eutectic under the prevailing cooling rate for the thermal cups that were used. Figure 9-a presents the macrostructure of sample #14 which was used as an example. It shows a characteristic columnar structure that has developed from the surface towards the center. The columns consist of cementite and ledeburite plates (Figure 9-b) with embedded dendrites (coarse features in dark contrast in the micrograph). The orientation of these dendrites appears to be random, indicating that they nucleated and developed in the liquid ahead of the columnar front before it captured them. In Figure 9-c, a few cells with very small graphite precipitates can be seen that are also aligned between the columns of the

metastable eutectic, suggesting that they formed behind or along with the columnar solidification front.

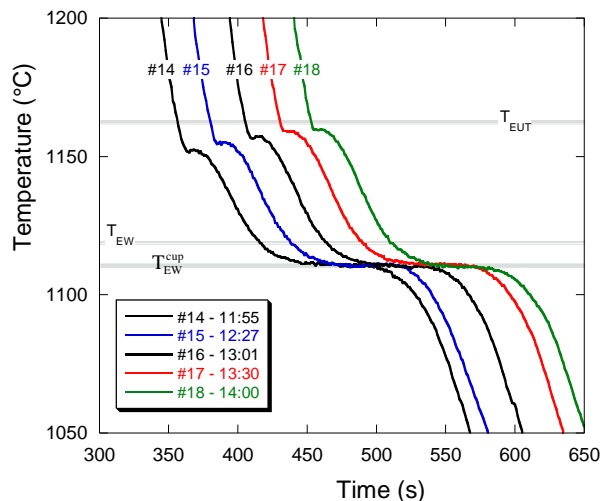


Figure 8. Temperature-time records of samples #14 to #18 shifted along the X axis for clarity.

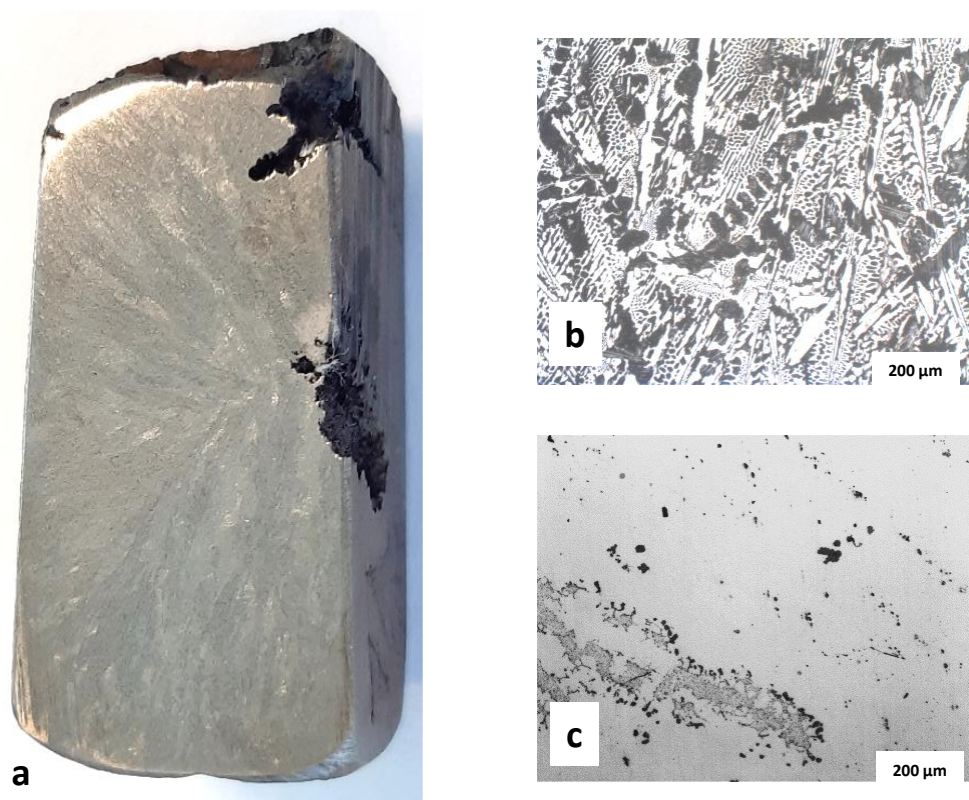


Figure 9. Metallographic observations of sample #14. a) Light macrophotography of half the vertical section of the etched sample whose height is 40 mm. b) and c) Light micrographs in the central area, after and before etching, respectively. In b, alignments of dendrite arms in dark contrast are seen to be randomly oriented.

The sharp transition in Figure 5-b indicates that the columnar structure in Figure 9 has developed with a nearly flat solidification front as already described by Mampaey [30]. In such a case, the latent heat released by the metastable eutectic is removed by the solid rim and does not lead to recalescence in agreement with the observation of very flat eutectic plateaus. Furthermore, the growth occurs at nearly constant temperature -i.e., at nearly constant undercooling with respect to the  $T_{EW}$ - that is imposed by the heat flow. Finally, it is noteworthy that these records show a slight recalescence of the  $T_{LA}$  arrest in contrast to all previous records, #1 to #13. This is in agreement with the nucleation and growth of austenite dendrites ahead of the columnar front that was mentioned above, and in this case heat is extracted by the liquid generating some recalescence. On the contrary, the austenite dendrites should have been part of the solidification front when well-defined cells of stable eutectic developed as no recalescence was noticed.

### 3.2 Tellurium-rich precipitates

To complement the thermal analysis results presented in Section 3.1, an attempt was made to investigate the presence of Te-rich zones in samples #9, #10, #14 and #17. As a first step, the coating applied to the thermal analysis cups was examined and found to consist of pure tellurium particles embedded in a silicate matrix, Figure 10. Chemical analysis of the coating indicates 26-27 wt% Te. A somewhat similar coating (20% Te, 10% clay, and 70% water, by weight) was defined and used by Decrop [33] for comparison with the usual direct melt addition method known to give erratic recovery results [34]. For better reproducibility of melt addition, Zirbo proposed to introduce Te into the melt using a copper or cast iron capsule [35]. However, for thermal analysis, Te-coated cups certainly give the most reproducible results.

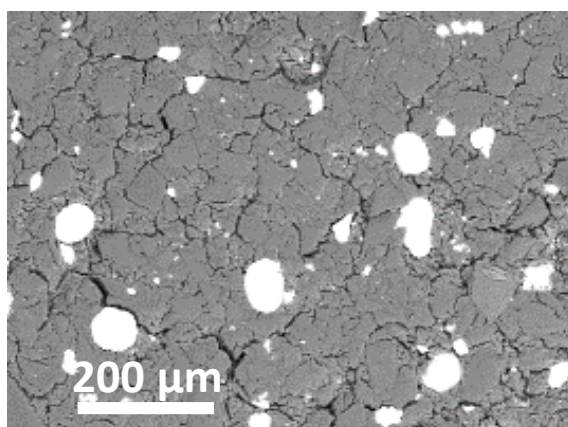


Figure 10. SEM micrograph of the Te coating.

Due to the constitution of the coating, it is not surprising that pure Te particles could be observed in the cast samples. These particles are the remnants of those present in the coating that were not completely dissolved. They were found in the metastable and stable eutectics, as illustrated by the micrographs in Fig. 11. It is perhaps fortuitous to observe such particles in contact with graphite, since tellurium is supposed to inhibit the growth of graphite.

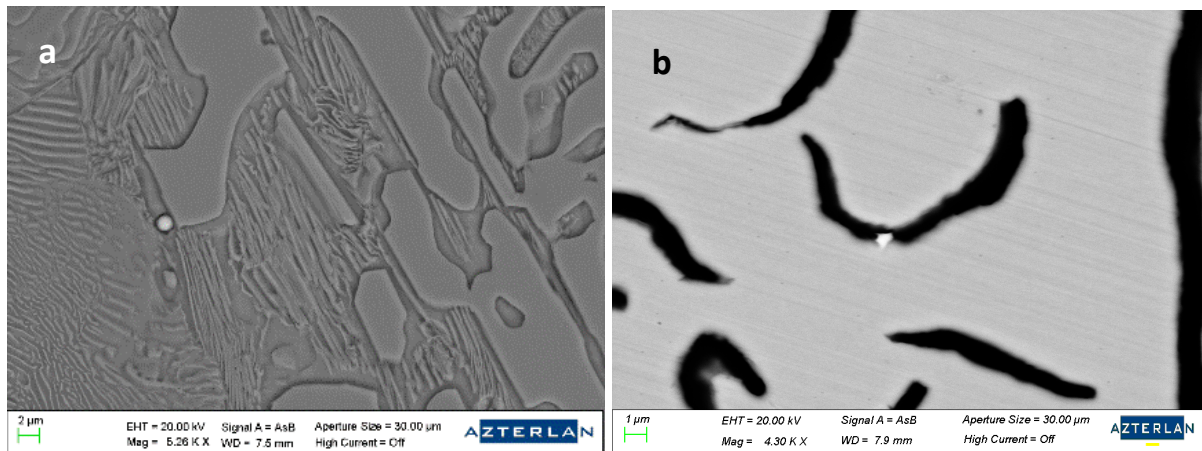


Figure 11. Te particles found in (a) an area with cementite (sample #9) and (b) an area with graphite particles (sample #10).

In some cases, the pure Te particles were associated with one or more other phases. In the example shown in Figure 12, the EDS spectrum revealed the presence of Ce and Ti in the vicinity of a bright spherical precipitate of pure Te. From these initial observations in Figures 11 and 12, it can be concluded that the particle size of Te in the coating is defined to provide an efficient tellurium yield when the melt is poured into the cup, i.e., to provide a good balance between dissolution rate and vapor loss.

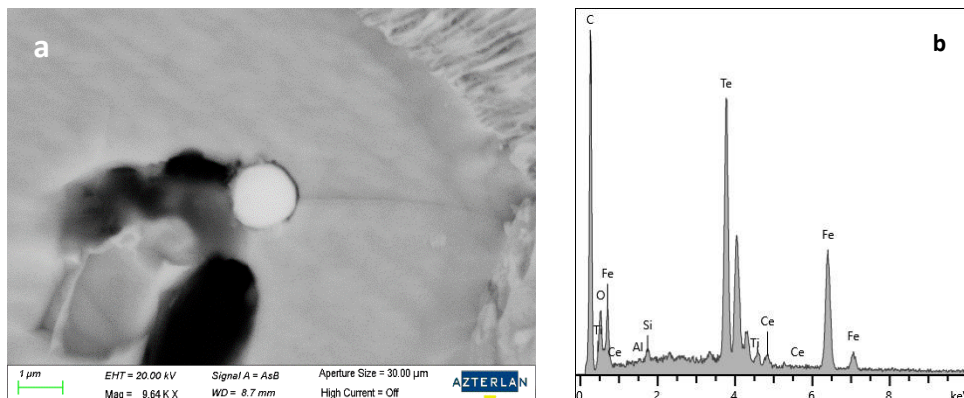


Figure 12. Rounded Te particle in contact with a small graphite particle in sample #10 (a) and associated EDS spectrum showing the presence of Ce and Ti bearing phases (b).

Other examples of multiphase precipitates that developed around pure Te particles are offered in Figure 13. In Figure 13-a, a square-shaped TiN precipitate enveloped the Te particle and formed a eutectic-like structure on the right side with a Mg-rich compound that was probably MgS although the S signal was weak. In Figure 13-b we see a TiN particle with the same characteristic square shape as in Figure 13-a with tiny Te-rich particles located near the hole in the middle. The EDS spectrum in the hole showed no major elements other than C, Te and Ti, suggesting that it was occupied by graphite that spalled off during metallographic preparation. If this was the case, then the TiN precipitate appeared after the graphite particle during solidification, with the Te particles in contact with the graphite precipitate as in Figure 11-b.

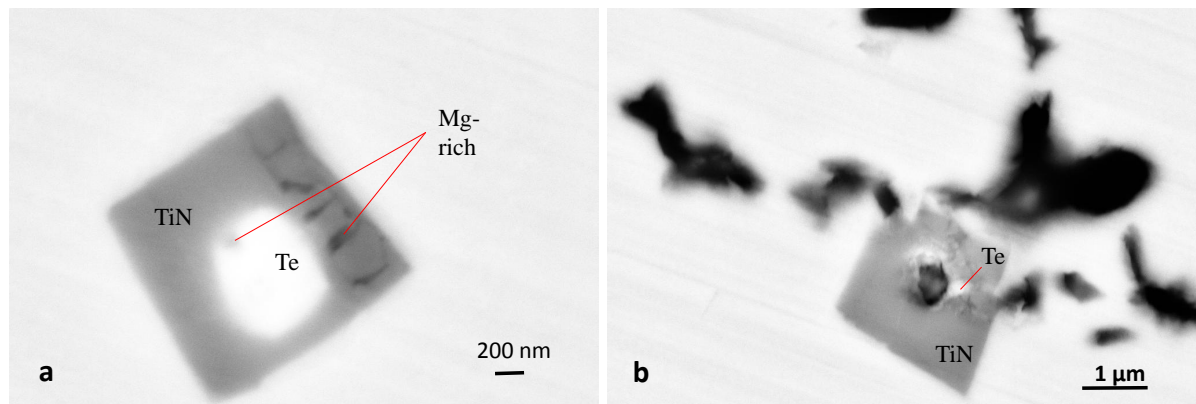


Figure 13. SEM micrographs of sample #10 showing two TiN precipitates with embedded Te particles (a and b).

Other Te-rich compounds that contained also Mg, Mn, as well as S for some of them, were observed associated with other phases as illustrated in figures 14 and 15. In the figures, they have been labeled as Te,Mg,Mn or Te,Mg,Mn,S particles. The round precipitate at the upper right of Figure 14-a shows two levels of bright contrast with a reentrant angle indicative of the presence of two different phases. The EDS spectrum showed Te, Mg, Mn and a low level of S, suggesting the brightest part of the precipitate contained Te, Mg and Mn, while the less bright upper part contained also S. On the periphery, small dark spots have been tentatively identified as MgS precipitates. Ti and N were apparently rejected from these phases and led to the formation of a TiN precipitate.

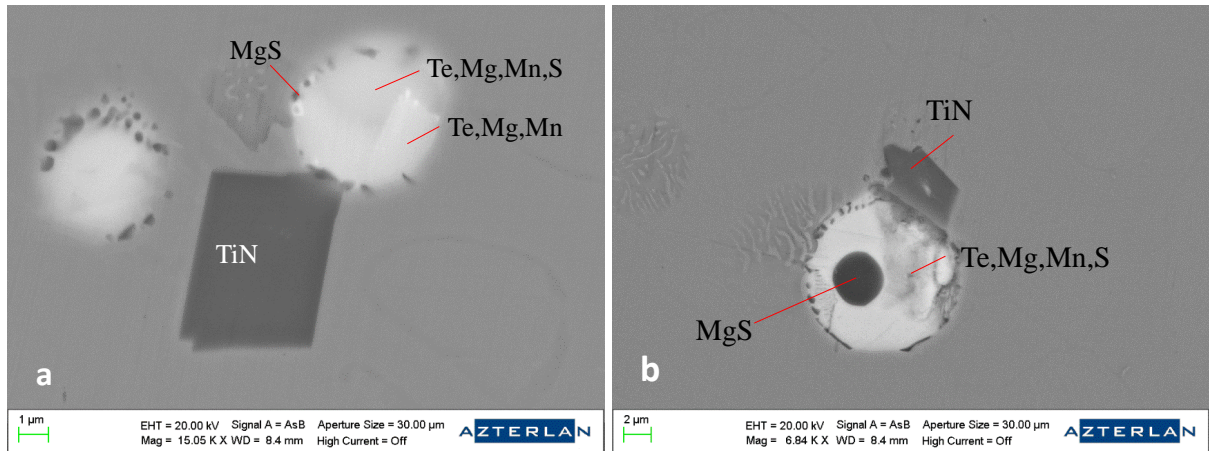


Figure 14. Examples of multi-phase particles showing Te associated with Mg, Mn and S in Sample #14 (a and b).

The same two brightness levels of Te-rich precipitates can be seen in the other examples in Figures 14-b and 15-a. Figure 15-a shows an example where Ti was not detected by EDS and no TiN precipitate could be found while the other two examples, Figure 14-b and Figure 15-b, show TiN precipitates as in Figure 14-a. Finally, it is interesting to note that MgS (Figure 14-b) or MgO (Figure 15-b) appeared in a central location with Te-rich precipitates around them, suggesting that these different phases have coalesced.

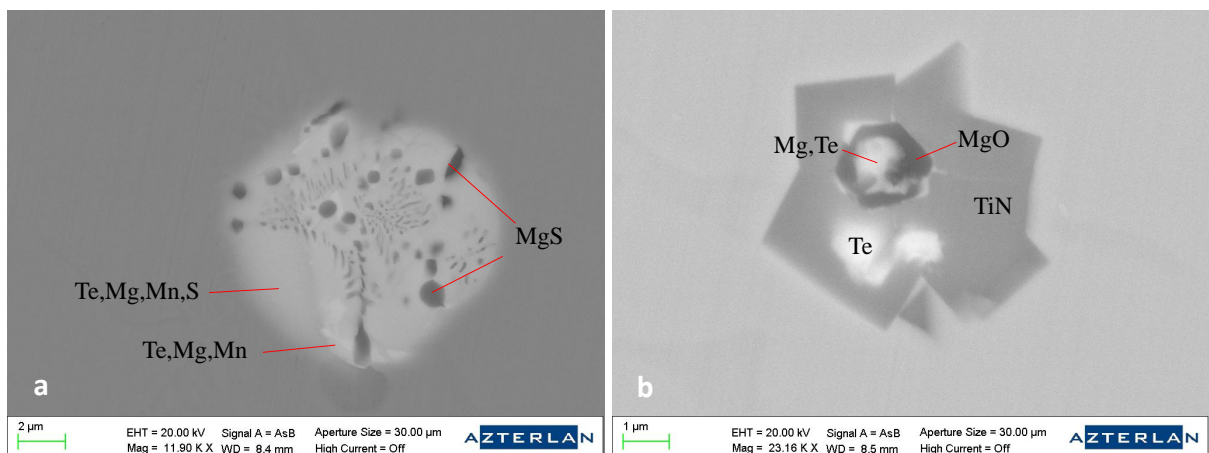


Figure 15. Examples of multi-phase particles showing Te associated with Mg, Mn and S in sample #17 (a and b).

To supplement these observations, the tellurium content of samples #10 and #17 was measured by chemical analysis, from both the carbide and the graphitic parts of these pieces. The total tellurium content was not sensitive to the type of microstructure but seemed to depend on the magnesium content. This was verified with measurements made on another set

of castings that were processed following the same procedure than in the present work, and the results are shown in Figure 16 as the total tellurium content versus the total magnesium content. This strong relationship suggests that the more Te and Mg combine during filling and solidification of thermal analysis cups, the less tellurium is lost to evaporation.

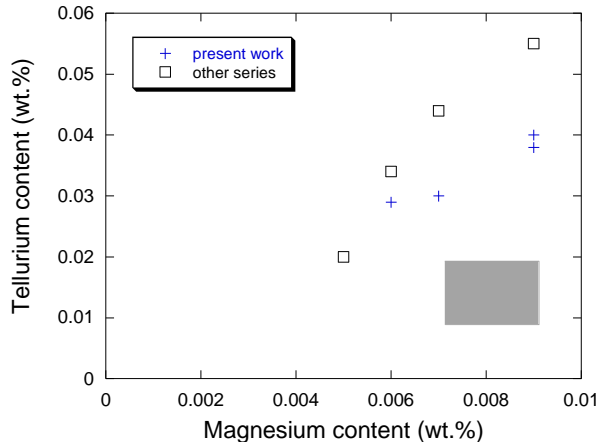


Figure 16. Relation between total tellurium and total magnesium in samples from the present work and from another series of castings. Magnesium contents are given at  $\pm 0.001$  wt.% and tellurium contents at better than  $\pm 0.005$  wt.%, both for a confidence interval at 95%. This maximum uncertainty is represented with the greyed rectangle at the bottom right in the figure.

#### 4. Discussion

This discussion is dedicated in a first part to the role of tellurium upon cast iron solidification at decreasing magnesium level. The second part stresses the consequences of the present work on the use of thermal analysis.

##### 4.1. Effect of the Mg/Te ratio upon solidification of cast iron.

It has long been considered that S, Se, and Te should have a similar effect on cast iron solidification due to their proximity in the periodic table [36], while the subtle differences between these elements are still being investigated [37]. They also share similar risk concerns [38]. For the same reason, and based on industrial practice, Aborn considered that Bi should have similar effects to Se and Te [34] in steels where they form round and discrete precipitates that facilitate machining, and in cast irons to promote metastable solidification. In effect, Bi, Se and Te share with S the fact that they are surface active on molten iron [39, 40] and lead to a liquid miscibility gap, although it is metastable in the Fe-S binary system. This

miscibility gap explains the formation of round particles in steels and certainly also the roundness of Te and Te,Mg,Mn,S particles described in the previous section.

Quantitative comparison of the effect of Bi and Te in non-spheroidized melts has confirmed that the latter is much more effective than the former, see for example Surendra et al. [41]. 20 to 40 ppm of Te in the melt are effective in obtaining cast irons containing only metastable eutectic for a silicon content of less than 2 wt.% [42]. Moreover, Te is interesting for this so-called whitening effect because it does not affect the graphitization step during malleabilization [42]. The effect of the elements Bi, Se and Te on the transition between stable and metastable eutectic solidification of non-spheroidal cast irons can be understood by considering that these additions limit the growth of graphite and therefore increase the solidification undercooling [7, 17]. As a result, at an intermediate addition level, eutectic solidification would proceed at a fairly low temperature, albeit above  $T_{EW}$ , leading to undercooled or mesh graphite as in Figure 4-a. By adding 20 to 200 ppm Te to cast irons with 2.5 and 5 wt.% Si, Dawson was able to obtain aggregate-nodular graphite at low carbon content, as well as mesh graphite at high carbon content [28]. This author associated the formation of nodular-type graphite with high undercooling, especially when the Te content was increased above 20 ppm and more and more metastable eutectic was obtained.

Magnesium treatment also is known to decrease the eutectic temperature, although this element does not inhibit graphite growth as much as Bi, Se and Te. In all cases, the increase in undercooling increases the carbon supersaturation of the liquid and thus triggers the activation of substrates for graphite nucleation. In this regard, bismuth has been shown to increase the number of nodules in spheroidal graphite cast irons when added as pure metal, oxide or sulfide or in an inoculant, and Bi-rich particles have indeed been observed in the center of graphite spheroids [43-46]. Similarly, Alonso et al. [47] have studied the effect of addition of Se to a spheroidized melt and observed that some of the graphite nuclei did contain Se and rare earth rich phases. Nodule count was also found higher on the samples cast with addition of Se as compared with the same sample without addition and the authors concluded that addition of Se triggers the formation of graphite nuclei. Similarly, Te has been found in graphite nuclei, associated with Mn and S and some limited amounts of Mg and Ce [32] or with oxygen and rare earths [48]. Tsutsumi et al. [17] mention also Japanese works that have reported Mn-S-Te compounds and oxides acting as nuclei in Te-doped cast irons. More recently, Saito et al. [49] reported that 10-20 ppm of tellurium (measured on the alloys)

increases the nodule count of spheroidized melts, and stressed that the most effective amount depends on the magnesium content and is only little below the critical level for graphite degeneracy (low Mg level) or carbide precipitation (high Mg level).

The above discussion helps to understand the evolution of the eutectic characteristics during the 8-hour test as observed in the present work. Figure 17 shows the evolution as a function of the number of castings of the total magnesium content measured by chemical analysis. During the first nine castings, the tellurium incorporated in the melt is consumed by the precipitation of Te-Mg-Mn-(S) phases, leading to a free magnesium content lower than the total magnesium content, as suggested by the thin vertical arrow. During this stage, there is no free tellurium in the liquid to prevent graphite growth which is thus controlled by the free magnesium. From casting #10 to casting #18, the total magnesium content continues to decrease and is now totally consumed by tellurium. Consequently, the amount of free tellurium increases more and more, probably acting first to form graphite nuclei (castings #10 to #13) but also to prevent the growth of graphite. This second effect becomes fully effective from casting #14 when the eutectic transformation proceeds fully in the metastable system.

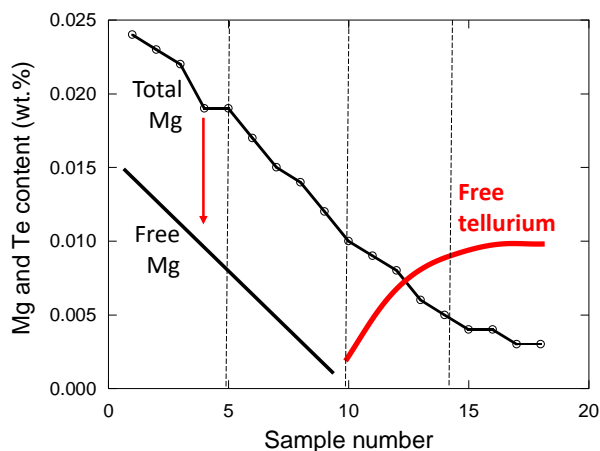


Figure 17. Evolution of total Mg, free Mg and free Te contents with the sample number (time). The total magnesium content was measured while the free magnesium and free tellurium are indicative and not to scale. The dashed vertical lines separate the four stages defined in relation with figure 1.

#### 4.2. Consequences on thermal analysis of cast irons.

Owing to the addition of Te, it was expected that solidification would have proceeded in the metastable system. As a matter of fact, it seems effectively that many of the samples started

their solidification with precipitation at the surface of the cups of a columnar outer zone consisting possibly of some austenite dendrites but mostly of metastable eutectic. The temperature of this metastable eutectic front must have been below  $T_{EW}$  by an amount dependent on its growth rate. During this early growth, heat was continuously extracted from the liquid through the solid rim and, after some time, the temperature differences in the remaining liquid levelled off as shown in the literature by a number of simultaneous records with one thermocouple at the center and one other located away from the center [12, 50, 51]. During this cooling, the central thermocouple recorded an arrest associated with the formation of austenite and the shape of the record below  $T_{LA}$  then depended on the fact that graphitic cells did or not nucleate and grow in the remaining liquid.

If no graphitic cells have formed, then the liquid has completely solidified as a metastable eutectic with the heat extracted through the columnar rim, leading to a eutectic plateau without recalescence. If many graphitic cells appeared, then enough heat was generated in the liquid whose temperature could rise again, showing a significant recalescence. However, many intermediate cases may appear depending on the number of stable eutectic cells. In all cases where a stable eutectic has appeared, it can be stated that the temperature of any flat part of the eutectic plateau is higher than the expected  $T_{EW}^{cup}$  value for the metastable eutectic as was the case of sample #4 (see figure 3). A critical case was identified with casting #7 which showed a completely flat eutectic plateau while the microstructure in the central part of the sample was graphitic.

## 5. Conclusion

When a melt that has been spheroidized with magnesium is held at high temperature, its magnesium content decreases leading to lower number of graphite nuclei and to a change of graphite shape to compacted graphite. With increased holding time, the temperature for the eutectic transformation decreases until the metastable eutectic replaces the stable one. Adding low level of tellurium to the melt by casting it in Te-coated cups for thermal analysis does accelerate the process because of the formation of Te-Mg compounds. However, these compounds can also act as graphite nuclei so that the transition to solidification in the metastable system is not complete. As the amount of magnesium is further decreased by longer holding of the melt, these Te-Mg compounds replace the original Mg compounds and the alloy solidifies again in the stable system. Finally, further decrease of magnesium leads to

more and more tellurium dissolved in the melt that acts as graphite impeder thus allowing for a fully metastable solidification. Thus, this is only when the amount of magnesium is high enough to tight all the tellurium that a control of the magnesium content could be envisaged.

This ambivalent role of tellurium, namely impeding graphite growth when dissolved in the melt but nucleating graphite when tight as Te-Mg compound, led to a large variety of cooling curve records in the present study. In the transition zone, between more Mg than Te and more Te than Mg, unreliable thermal analysis records showed a plateau with a flat part usually associated to metastable solidification but related here with a mixed microstructure consisting of an outer rim of metastable eutectic and an inner material having solidified in the stable system.

### Acknowledgments

This research did not receive any specific grant from funding agencies in the public, commercial, or not-for-profit sectors.

### References

- [1] U. de la Torre, J. Sertucha, A. Regordosa, J. Lacaze, Effect of silicon on the metastable eutectic temperature of Fe-C-Si alloys, to appear in Metall. Mater. Trans. B
- [2] M. Hillert, Phase equilibria, phase diagrams and phase transformations, University Press, Cambridge, 1998
- [3] E. Fraš, H.F. Lopez, M. Kawalec, M. Gorny, Role of alloying additions in the solidification kinetics and resultant chilling tendency and chill of cast iron, Metals 5 (2015) 256-288.
- [4] P. Magnin, W. Kurz, Competitive growth of stable and metastable Fe-C-X eutectics: Part I. Experiments, Metall. Trans. A 19 (1988) 1955-1963.
- [5] P. Magnin, W. Kurz, Competitive growth of stable and metastable Fe-C-X eutectics: Part II. Mechanisms, Metall. Trans. A 19 (1988) 1965-1971.
- [6] P. Magnin, R. Trivedi, Eutectic growth: a modification of the Jackson and Hunt theory, Acta metal. Mater. 39 (1991) 453-467.
- [7] J.D. Verhoeven, J.S. Park, L.L. Jones, Effect of Te on morphological transitions in Fe-C-Si alloys: Part I. Directional solidification, Metall. Trans. A 20 (1989) 1867-1873.
- [8] J.D. Verhoeven, A.J. Bevolo, J.S. Park, Effect of Te on morphological transitions in Fe-C-Si alloys: Part II. Auger analysis, Metall. Trans. A 20 (1989) 1875-1881.

- [9] M. Hillert, V.V. Subba Rao, Grey and white solidification of cast iron, ISI Pub. 110 (1969) 204-212.
- [10] A. Moore, Carbon equivalent of white cast irons, AFS Cast Metals Res. J. March (1972) 15-19.
- [11] R.W. Heine, Liquidus and eutectic temperatures and solidification of white cast irons, AFS Trans. 85 (1977) 537-544.
- [12] V. Anjos, R. Deike, C.S. Ribeiro, The use of thermal analysis to predict the dendritic coherency point on nodular cast iron melts, Cienca & Tecnologia dos Materiais 29 (2017) e27-e33.
- [13] D. Stefanescu, R. Suarez, Sung Bin Kim, 90 years of thermal analysis as a control tool in the melting of cast iron, China Foundry 17 (2020) 69-84.
- [14] E Fraš, HF Lopez, A theoretical analysis of the chilling susceptibility of hypoeutectic Fe-C alloys, Acta metall. mater. 41 (1993) 3575-3583.
- [15] L. Nastac, D.M. Stefanescu, Modeling of the stable-to-metastable structural transition in cast iron, Adv. Mater. Res. 4-5 (1997) 469-478.
- [16] H. Nieswaag, A.J. Zuithoff, Solidification structures and graphite patterns in tellurium-treated grey cast iron, 34<sup>th</sup> International Foundry Congress, 1967, paper 19
- [17] N. Tsutsumi, M. Imamura, M. Nakada, The influence of tellurium on the graphite formation of cast iron during solidification, report 28 of the Castings Research Laboratory, Waseda University, 1977
- [18] W. Oldfield, The chill-reducing mechanism of silicon in cast iron, BCIRA J. 10 (1962) 17-27.
- [19] A. Regordosa, J. Lacaze, J. Sertucha, M.J. Castro-Roman, U. de la Torre, O. Dezellus, Is thermal analysis able to provide carbon and silicon contents of cast irons?, Int. J. Metalcasting (2022) DOI: 10.1007/s40962-022-00799-5
- [20] A. Regordosa, U. de la Torre, A. Loizaga, J. Sertucha, J. Lacaze, Microstructure changes during solidification of cast irons: effect of chemical composition and inoculation on competitive spheroidal and compacted graphite growth, Int. J. Met., 14 (2020) 681-688.
- [21] A. Regordosa, U. de la Torre, J. Sertucha, J. Lacaze, Quantitative analysis of the effect of inoculation and magnesium content on compacted graphite irons – Experimental approach, J. Materials Processing and Technology 9 (2020) 11332-11343.
- [22] M. Castro, M. Herrera, M. M. Cisneros, G. Lesoult, J. Lacaze, Simulation of thermal analysis applied to the description of the solidification of hypereutectic SG irons, Int. J. Cast Met. Res. 11 (1999) 369-374.

- [23] W. Oldfield, J.G. Humphreys, Formation of nodular graphite in hypo-eutectic irons, BCIRA J. 10 (1962) 315-324.
- [24] M. J. Castro-Román, J. Lacaze, A. Regordosa, J. Sertucha, R. del Campo-Castro, Revisiting Thermal Analysis of Hypereutectic Spheroidal Graphite Cast Irons, Metall. Mater. Trans. A 51 (2020) 6373-6386.
- [25] J. Lacaze, A. Regordosa, J. Sertucha, U. de la Torre, Quantitative analysis of solidification of compacted graphite irons – A modelling approach, ISIJ Int. 61 (2021) 1539-1549.
- [26] J.C. Sawyer, J. F. Wallace, Effects and Neutralization of Trace Elements in Gray and Ductile Irons - Part 1. AFS Trans. 76 (1968) 386-404.
- [27] J. Tybulczuk, Y Nakano, Y. Kawano, W. Sakwa, J.C. Margerie, Etude sur les formes dégénérées du graphite, Fonderie 355 (1976) 123-138.
- [28] J.V. Dawson, Formation of nodular graphite structure by tellurium in cast iron, AFS cast metals research J. September (1970) 111-113.
- [29] J.V. Dawson, Effects of selenium and tellurium on the structure of cast irons and their dependence on hydrogen content, AFS Trans. 77 (1969) 113-120.
- [30] F. Mampaey, Solidification morphology of white cast iron, AFS Trans., 2003, paper 68
- [31] V.M. Gobinath, K. Annamalai, Experimental investigation of Te addition on chilled cast iron tappet manufacturing process, Mater. Manuf. Process. 36 (2021) 1299-1304.
- [32] H. Nieswaag, A.J.Zuithoff, The occurrence of nodules in cast iron containing small amounts of tellurium, AFS Cast Metals Research J. December (1971) 165-171.
- [33] M. Decrop, Quelques remarques sur la trempe primaire des fontes, Fonderie 246 (1966) 299-316.
- [34] R.H. Aborn, The role of selenium and tellurium in ferrous metals, Proc. Of the symposium on Metallurgy of substitute ferrous and non-ferrous alloys, National Metallurgical Laboratory (NML), Jamshedpur, India, 1966, pp. 342-343.
- [35] G. Zirbo, Influence du tellure sur la structure de la fonte grise, Fonderie 309 (1972) 43-48.
- [36] S. Garber, The effects of Sulphur, selenium, and tellurium on graphite formation in an Fe-C-Si alloy, J. Iron Steel Inst. 181 (1955) 291-302.
- [37] J. Ibers, Tellurium in a twist, Nature Chemistry 1 (2009) 508.
- [38] E.S. Blackadder, W.G. Manderson, Occupational absorption of tellurium: a report of two cases, British J. Industrial Medecine 32 (1975) 59-61.

- [39] K.I. Vashchenko, K.K. Kosnyanu, V. Ya. Zhuk, Surface tension of cast irons with different carbon equivalents and the influence thereon of bismuth additions, Russian Casting Production (1966) 72-74.
- [40] K. Ogino, K. Nogi, O. Yamase, Effects of selenium and tellurium on the surface tension of molten iron and the wettability of alumina by molten iron, Trans. ISIJ 23 (1983) 234-239.
- [41] Y. Surendra, H.M.D. Roshan, V. Panchanathan, Effect of small additions of tellurium & bismuth on the white iron formation tendency, Indian Journal of Technology 11 (1973) 709-712.
- [42] W. L. Hallerberg, J. F. Wallace, Effects and neutralization of trace elements in malleable iron – Part 2. AFS Trans. 76 (1968) 405-416.
- [43] H. Horie, T. Kowata, A. Chida, Influence of bismuth on graphite nodule count in thin-section spheroidal-graphite cast iron, Cast Metals 2 (1990) 197-202.
- [44] H. Takeda, H. Yoneda, K. Asano, Effect of silicon and bismuth on solidification structure of thin wall spheroidal graphite cast iron, Mater. Trans. 51 (2010) 176-185.
- [45] P. Ferro, A. Fabrizi, R. Cervo, C. Carollo, Effect of inoculant containing rare earth metals and bismuth on microstructure and mechanical properties of heavy-section near-eutectic ductile iron castings, J. Mater. Proc. Technol. 213 (2013) 1601-1608.
- [46] H. Tsuji, H. Chono, N. Yamamoto, T. Kai, Y. Igarashi, Analysis of graphite nuclear in spheroidal graphite cast iron and mechanism of nodule count increase by Bismuth Oxide, Mater. Trans. 62 (2021) 1393-1400.
- [47] G. Alonso, D.M. Stefanescu, E. Aguado, R. Suarez, The role of selenium on the formation of spheroidal graphite in cast iron, Metals 11 (2020) 1600.
- [48] G. Alonso, D.M. Stefanescu, B. Bravo, E. Aguado, R. Suárez, Effect of tellurium on the nucleation process of spheroidal graphite in cast iron, J. Mater. Res. Tech. 19 (2022) 4451.
- [49] R. Saito, T. Nakamura, T. Maruyama, H. Yanagitani, T. Sakai, K. Nakamoto, Influence of tellurium addition to spheroidal graphite cast iron on the number of graphite particles, Int. J. Metalcasting, 13 (2019) 571-577.
- [50] E. Fras, W. Kapturkiewicz, A.A. Burbielko, H.F. Lopez, Numerical simulation and Fourier thermal analysis of solidification kinetics in high-carbon Fe-C alloys, Metall. Mater. Trans. B 28 (1997) 115-123.
- [51] A. Dioszegi, J. Hattel, Inverse thermal analysis method to study solidification in cast iron, Int. J. Cast Metals Res. 17 (2004) 311-318.